



An investigation to study the combined effect of different infill pattern and infill density on the impact strength of 3D printed polylactic acid parts

Pradeep Kumar Mishra, P. Senthil*, S. Adarsh, M.S. Anoop

Department of Production Engineering, National Institute of Technology, Tiruchirappalli, 620015, India



ARTICLE INFO

Keywords:

Additive manufacturing
Fused deposition modeling
Impact strength
Izod impact testing

ABSTRACT

The emanation of 3D printing technology has enabled researchers to manufacture complex geometrical structures to design high impact energy-absorbing structure for different laboratory and industrial applications. In the present investigation, an Impact test had been performed to measure the absorbed energy during the plastic deformation of the PLA (Polylactic acid) 3D printed components with the combination of different infill patterns and infill densities. Experimental investigation on specimens through the Izod impact test concluded that at 85% infill density for each infill pattern, the energy absorption is maximum. Results showed that the fracture resistance of specimens was a mutual function of induced stress and crack propagation at the notch area during the impact test and the dynamics of impact failure outlined by mechanics of laminate composite.

1. Introduction

The market for the design of durable polymeric structures has grown significantly in many fields, such as sports, automobile, biomedical, packaging and civil, etc. [1–3] today. Thus, several experiments have been carried out on those sections to build such a structure to make them light with enhanced strength and resistance to impact. Such kinds of resilient structures often provide the engineer or researcher with the challenge of designing and manufacturing the component to meet design requirements. Due to the flexibility of the FDM (fused deposition modeling) process in making the mesostructure, this problem can be easily solved by printing different densities of infill (packing density) and patterns to establish the optimum structure. The FDM process was primarily used for prototyping by manufacturers, but due to the advent of manufacturing techniques and the use of fiber-reinforced plastics as filaments, the process can print load-bearing components with the resistance to higher strain rate [4]. The arrangement of rasters and layers in the FDM process forms a structural framework otherwise called mesostructure, and the G. Alaimo et al. reported that it had a significant impact on the mechanical properties of the components [5]. Many process parameters control the functional properties of the component manufactured by the FDM process and among them air gap, layer thickness, raster angle, raster width, infill density and build orientations play a crucial role in influencing those properties [6,7,8]. (see Tables 1 and 2)

O. S. Es-Said et al. [9] found that compared with other raster orientations, parts in which the raster orientations are parallel to the loading axis showed higher tensile stiffness and bending stiffness. A. Tsouknidas et al. [10] studied the impact of layer height on the dissipating energy characteristics of the printed PLA structure and found that an increase in layer height increased the risk of premature failures. As the layer height increases, the increased distance between the neighboring beads raises the level of stress concentration during impact loading. Compared to the thicker layer, the thinner layer takes more time to create the component, and the thinner layer holds a temperature above the melting point for extended period of time [11]. The shorter layer height, therefore, increased the impact strength by generating less stress concentration and building excellent diffusion bonds among the beads which ultimately improved impact resistance. Fillip Gorski et al. [12] investigated that compared to the same monolithic part generated by the injection moulding process, the impact strength of FDM-based samples decreased drastically. Tanveer et al. [13] measured the PLA specimen's impact strength at 50%, 70%, and 100% infill density, and considered the impact strength to be directly proportionate to infill density. The study predicted that due to the increase in material packing density in the specimen, the rise in impact resistance was observed and thus the stress intensity factor decreased. It was found from the above literature data that the impact resistance of the 3D printed structure is highly dependent on the mesostructure geometry. The mesostructure is a function of the density of infills and the pattern of infills in each

* Corresponding author.

E-mail address: senthil@nitt.edu (P. Senthil).

Table 1
Representation of different design mix for impact specimens.

Serial Number	Combination of different Infill pattern & Infill density	Number of Samples
1	Line {50, 75, 80, 85, 90, 95, 100}	7
2	Zig-zag {50, 75, 80, 85, 90, 95, 100}	7
3	Concentric {50, 75, 80, 85, 90, 95, 100}	7
4	Cross {50,75}	2
5	Cross 3D {50,75}	2
6	Concentric 3D {50,75}	2
7	Cubic subdivision {50,75}	2
8	Grid {50,75}	2
9	Octet {50,75}	2
10	Quarter Cubic {50,75}	2
11	Triangular {50,75}	2
12	Tri-hexagon pattern {50,75}	2

Table 2
Fixed process parameters for printing.

Serial Number	Printing parameters	Value
1	Layer height	0.2 mm
2	Initial layer height	0.2 mm
3	Line width	0.35 mm
4	Wall line width	0.35 mm
5	Outer wall line width	0.35 mm
6	Inner wall line width	0.3 mm
7	Wall thickness	1 mm
8	Wall line count	3
9	Printing temperature	215 °C
10	Build plate temperature	60 °C
11	Nozzle Flow	100%
12	Build plate adhesion type	None

component. Hence, its geometry can influence the propagation of cracks and the factor of stress intensity regarding impact loading and influence the impact strength of the component. The dynamics of failure due to impact load on specimens were described by the mechanics of laminated composite structure [20].

The reported resistance of the Izod impact is defined as this energy divided by the region of the mid-section. While there are inconsistencies in the calculations of energy dissipation due to the kinetic energy of broken specimens and multiple fractures and delamination, impact energy offers a useful calculation for comparative purposes at least. There

are very few investigations available to explain the function of the mesostructure in the propagation of cracks and the effect of stress intensity on the impact strength of the printed parts. For this purpose, specimens were printed with different combinations of infill densities and infill patterns (line, zigzag, concentric, cross, concentric 3d, cross 3d, cubic subdivision, circle, octet, quarter cubic, triangular, and tri-hexagon pattern) to research the effect of mesostructure. From the initial investigation it was found that line, zigzag and concentric exhibited excellent energy-absorbing capability impact over other patterns of infill. Therefore, the printing of infill patterns with multiple infill densities was confined to the line, zigzag and concentric patterns. Regarding the material selection for fabricating the specimen, the semi-crystalline polymer 'PLA' was preferred for investigation because of its remarkable biocompatibility and biodegradability characteristics [14].

The major objectives of the present investigation are:

- Representation of a significant impact energy dataset for multiple combinations of infill density and infill geometry pattern.
- Comparison of different infill density and geometry under the same experimental constraints.
- Discussion of the inferences on impact strength obtained from the experiment in the context of stress intensity and crack propagation.

2. Materials and methods

2.1. Design and manufacturing of samples

The impact specimen's 3D model (Fig. 1a) was developed in accordance with the ASTM D256 specification (Fig. 1b) in the CREO parametric solid modeling program, and a total of 117 specimens were selected from the combinations of infill density and infill pattern (Table-1). The specimens were manufactured using the FDM technique using PLA feedstock material in the 'Ultimaker 3 Extended' 3D printer according to the appropriate process parameters (Table –2).

2.2. Experimental set-up

For a given group of process parameters, each sample set consisted of three specimens. The results were taken as the mean impact strength values of the mechanical test. Since the physical properties of many materials (especially thermoplastics) can vary depending on ambient temperature, room temperature tests were performed according to the standards. Izod impact tests were performed to study the energy absorption and characterize the type of damage of the different configurations. The Izod impact strength test is a typical ASTM method of assessing material impact resistance. A pivoting arm (constant potential energy) (Fig. 2a) is raised to a specific height and then released. The arm swings down and reaches a notched sample and breaks the sample. The energy which the sample absorbs is determined from the height at which the arm swings after reaching the sample. The total energy of fracture is determined by

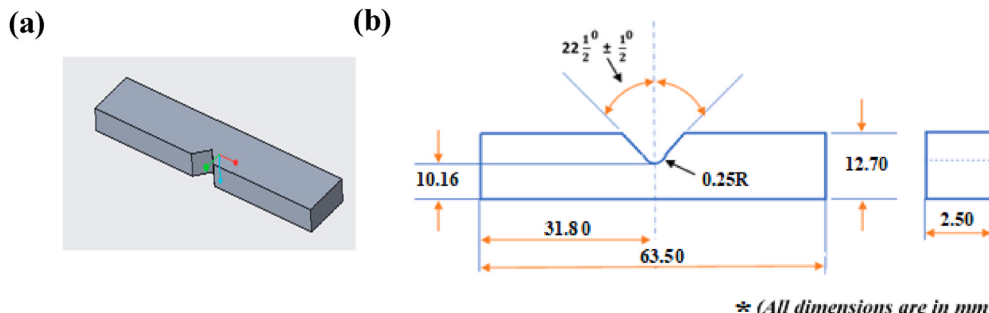


Fig. 1. (a) 3D model of Impact Test Sample and (b) Dimensions of Impact Test Sample according to ASTM D 256.

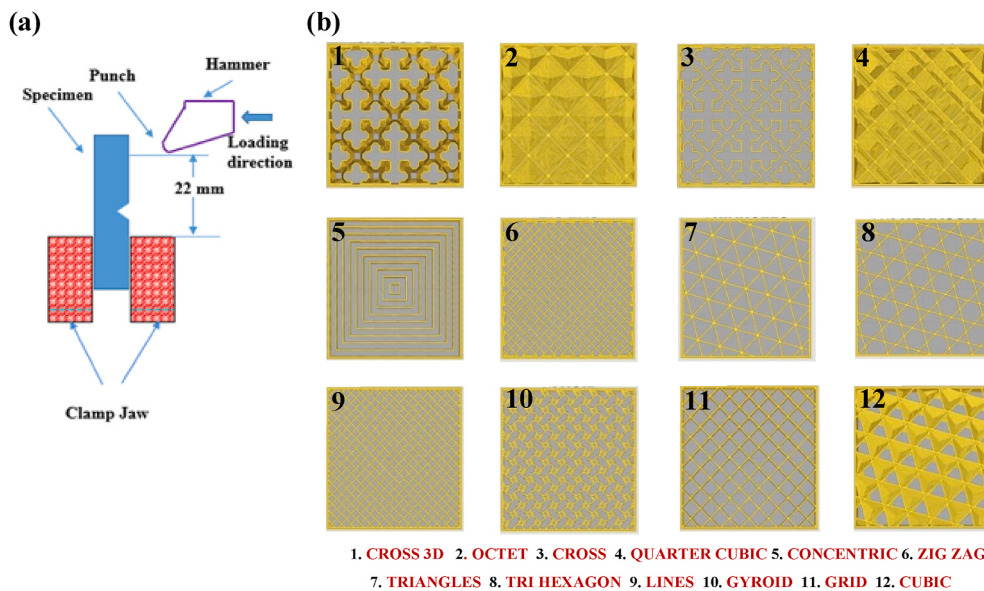


Fig. 2. (a) Schematic of impact testing equipment and (b) Geometrical arrangement of different infill patterns.

$$E_t = mg(h_o - h_f) \pm 1.5 J$$

where E_t is the total energy, m is the mass, g is gravitational acceleration, h_o is the original height and h_f is the final height. The absorbed energy per unit cross-sectional area (kJ/m^2) or impact strength E_c is defined as

$$E_c = \frac{E_t}{wt}$$

Where the width and thickness of the specimen are w and t , respectively. Owing to their limited contribution to the energy balance, energy losses due to bearing friction and air resistance were overlooked.

3. Results and discussion

The details of the impact resistance of all infill patterns are shown in Fig. 3a & b. As per the results the line, zigzag and concentric patterns are showing a better impact-resisting performance (Fig. 3a & b) as compared to others. Therefore, the focus of the investigation was restricted to test the combination of line, zigzag and concentric patterns (Fig. 2b) with infill densities (50%, 75%, 80%, 85%, 90%, 95%, and 100%). Information on energy absorption due to impact testing on different infill density combinations and patterns of 3D-printed PLA specimens are recorded in Fig. 4. The findings initially showed that there is a growing trend in the energy absorption of impacts as the percentage of infill density increases, but the trend decreases after 85% of infill volume, as shown in Fig. 4. As the mesostructure of the printed specimen plays a vital role in determining the factor of stress intensity and crack propagation and indirectly determining the force of impact. So, this study considered the mechanism of the element of stress intensity and the principle of crack propagation in the impact specimens for fracture analysis.

The mesostructure of the specimens was taken into consideration to explore the impact of stress intensity factor and crack propagation in the specimens. The line infill pattern was taken into the investigation for its basic geometrical topology and studied the impact of variance in the percentage of infill on stress intensity and propagation of cracks. Three percentages of infills (50%, 85%, and 100%) had been considered, and the mesostructure specifics are shown in Fig. 3c. For the case of infill density of 50%, the number of printing beads closer to the notch region is 14 numbers (other than the perimeter) as shown in Fig. 3c. Since the number of beads are smaller and there are large gaps in between printed beads, the higher stress induced by the impact load in the total cross-

section region and the stress-induced significantly. Furthermore, the higher porosity in the mesostructure of printed specimen limited the interfacial bonding strength among the beads and resulted in enhancing the fracture energy of specimen [21,22]. Therefore, this coupled factor drastically reduced the impact strength of specimens with 50% infill density. In the case of infill density of 85%, the number of beads is 23 closes to the specimen's notch as shown in Fig. 3c. The resisting region is more in this case, and the propagation of cracks is not constant through the geometry of the infill. This form of mesostructure thus absorbed a greater amount of energy from impacts, as shown in Fig. 4. The specimen printed with an infill density of 100% has 28 number of beads as shown in Fig. 3c. These 28 beads resist the impact effect, and each bead is in contact with the neighboring beads. The crack will easily propagate through the specimen once nucleated, as the resistant region is continuous (Fig. 5a & b). Thus, while the number of beads are more, the crack propagation rate moves rapidly and therefore the impact intensity has begun to decrease with each pattern of infilling.

The impact resistance result of each combination of infill density and pattern was carefully analyzed to prove the requirements for the crack propagation in the concern for the specimen's impact-absorbing ability. It is observed that zig-zag and concentric patterns from 50% to 85% infill density (Fig. 4) more follow the impact resistance of the infill line pattern. After that, the zig-zag pattern displayed greater impact-resistant capability than the other two patterns. At 100%, 95%, and 90% infill density, the line infill pattern specimens showed continuous crack propagation (Fig. 5a to c) at the surface region for which the fracture rate was high and eventually resulted in less impact power. In the case of the zig-zag pattern, the length of the crack is very long (Fig. 5b to d) compared to the pattern of line infill, and this delayed the rate of propagation of the crack. Hence this phenomenon leads to an enhancement of the zig-zag pattern effect resistance after infill density of 85% over the other two patterns. Compared to the line and the zig-zag infill pattern, the impact energy of the concentric pattern is lower for all infill density (Fig. 4). This is because sharp bends are present in a concentric pattern closer to the structure of the notch (Fig. 3d), which serves as a concentrator stress region. The specimen was exposed to more stress due to the presence of stress concentration zones and ultimately ended with less impact intensity relative to other infill patterns.

The impact resistance for all infill patterns showed the highest impact resistance value compared to other densities of infill at 85% infill density. At an infill density of 85%, some layer has undergone delamination (Fig. 5d) and this process reduced the fracture energy carried out

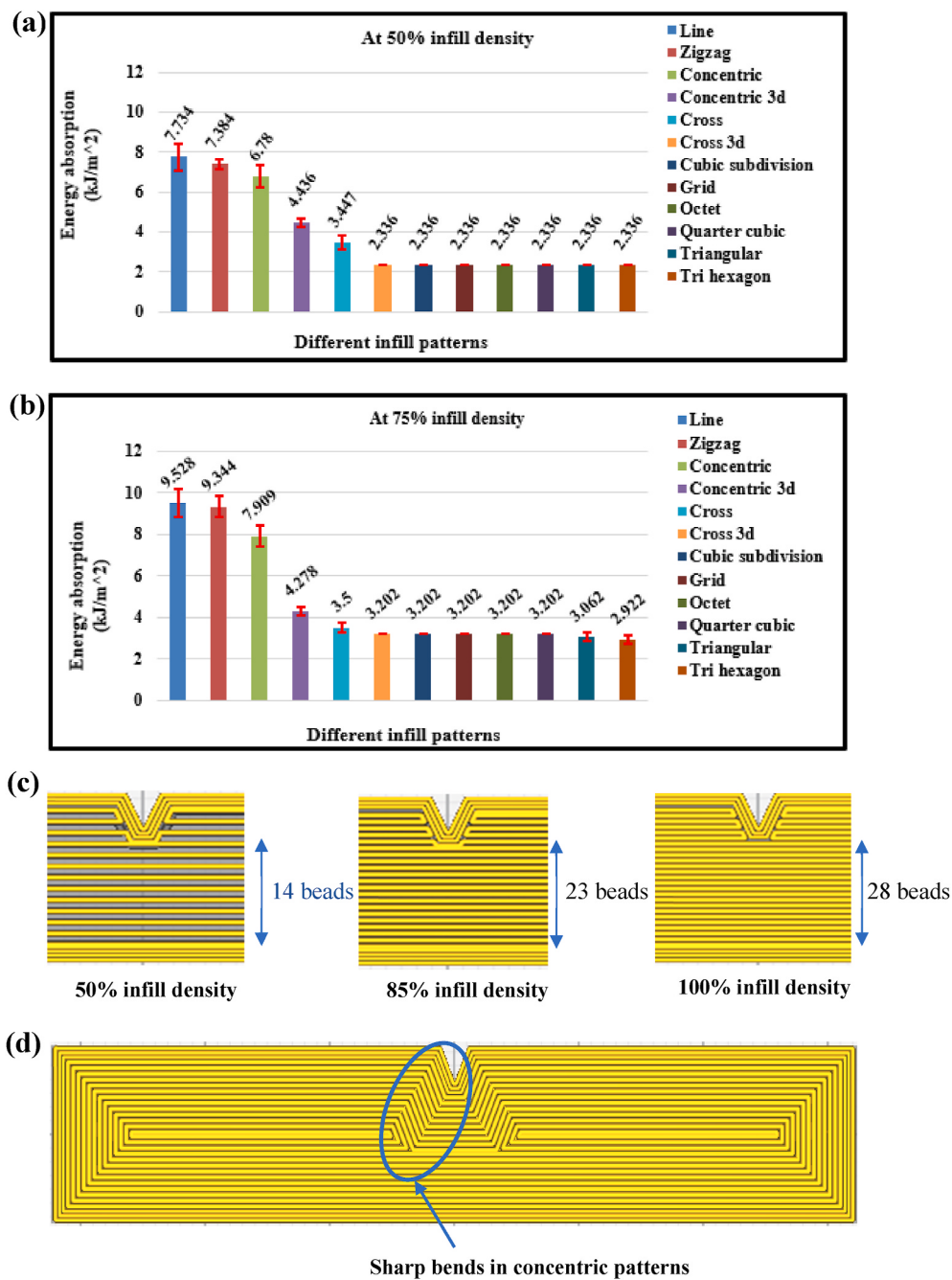


Fig. 3. (a) Energy absorption in specimen with various patterns at 50% infill density (b) Energy absorption in specimen with various patterns at 75% infill density (c) Mesostructure at different infill density of line pattern and (d) Mesostructure of concentric pattern showing sharp bends at notch zone.

by the crack tip and allowed a greater amount of energy to be absorbed by the specimens [15–19]. The difference between the maximum and minimum value of impact resistance at the infill density of 85% was about 55.07% and the difference value decreases as the value of infill density rises. The lowest difference value at 100% infill density was recorded to be 26.02% (Fig. 4). The result showed that the maximum impact resistance (13.91 kJ/m²) was recorded in the combination of 85% infill density and line infill pattern (Fig. 4) and this value was 3.49 times the impact resistance provided by neat PLA [17]. At 100% infill density, the crack length has almost the same magnitude for each infill pattern, and its impact resistance values have confirmed it (Fig. 4). This phenomenon showed that the specimens appear to be more homogeneous as infill density increases and crack is easily propagated through the notch field. In addition, at 100% and 95% infill density (Fig. 5a & b),

the delamination at the fracture zone disappeared in each infill pattern. Consequently, the impact resistance of specimens decreased sharply after the infill density of 85% and even dipped below impact resistance at 50%.

4. Conclusions

- It is observed that impact strength depends strictly on the nature of the mesostructure which plays the balance between the factor of stress intensity and the phenomenon of crack propagation. Thus, 85% demonstrated the highest energy absorbing potential across the infill density range (from 50 to 100%), with a combination of each infill template.

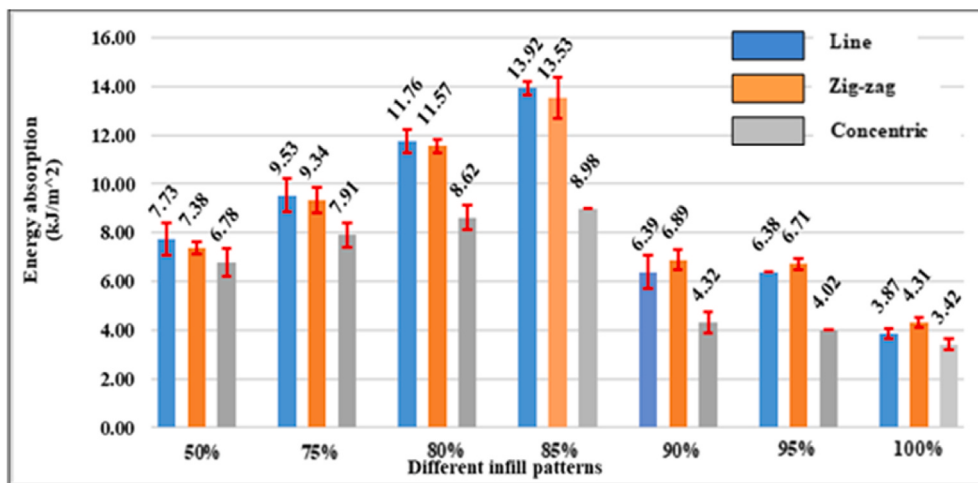


Fig. 4. Impact energy absorption at combination of different infill density and patterns.

- In the case of the concentric pattern, the stress concentration was a major drawback, which magnified the induced stress in the mesostructure for which structure fractured by consuming less energy compared to others.
- There is a gap between each printed bead in the specimen at lower infill densities (50%, 75%, 80%, and 85%). Thus, crack propagation in the infill pattern is not continuous and was resisted due to this crack nucleation, and the fracture was dominated by heavy stress due to limited surface area.
- The crack propagation catalyzed the rate of fracture at higher infill density (90%, 95%, and 100%), and this phenomenon occurred due to continuation in the resistant region in the specimen's mesostructure.
- Delamination of layers in mesostructure breaks the continuity of crack propagation during impact. This interruption of crack propagation, in the fracture region, gradually increases the structure's energy-absorbing ability.

Author statement

The authors declare that they have no known competing financial interests or personal relationships that could have appeared to influence the work reported in this paper.

Declaration of competing interest

The authors declare that they have no known competing financial interests or personal relationships that could have appeared to influence the work reported in this paper.

References

- S. Pina, J.M. Oliveira, R.L. Reis, Natural-based nanocomposites for bone tissue engineering and regenerative medicine: a review, *Adv. Mater.* 27 (2015) 1143–1169, <https://doi.org/10.1002/adma.201403354>.
- C. Ortiz, M.C. Boyce, Materials science: bioinspired structural materials, *Science* 319 (2008) 1053–1054, <https://doi.org/10.1126/science.1154295>.
- M.F.L. De Volder, S.H. Tawfick, R.H. Baughman, A.J. Hart, Carbon nanotubes: present and future commercial applications, *Science* 339 (2013) 535–539, <https://doi.org/10.1126/science.1222453>.
- P. Parandoush, D. Lin, A review on additive manufacturing of polymer-fiber composites, *Compos. Struct.* 182 (2017) 36–53, <https://doi.org/10.1016/j.compositesb.2017.08.088>.
- G. Alaimo, S. Marconi, L. Costato, F. Auricchio, Influence of meso-structure and chemical composition on FDM 3D-printed parts, *Compos. B Eng.* 113 (2017) 371–380, <https://doi.org/10.1016/j.compositesb.2017.01.019>.
- S.M. Sajadi, P.S. Owuor, R. Vajtai, J. Lou, R.S. Ayyagari, C.S. Tiwary, P.M. Ajayan, Boxception: impact resistance structure using 3D printing, *Adv. Eng. Mater.* 1900167 (2019) 1–10, <https://doi.org/10.1002/adem.201900167>.
- O.A. Mohamed, S.H. Masood, J.L. Bhowmik, Optimization of fused deposition modeling process parameters: a review of current research and future prospects, *Adv. Manuf.* 3 (2015) 42–53, <https://doi.org/10.1007/s40436-014-0097-7>.
- P. Kumar Mishra, P. S., Prediction of in-plane stiffness of multi-material 3D printed laminate parts fabricated by FDM process using CLT and its mechanical behaviour under tensile load, *Mater. Today Commun.* 23 (2020) 100955, <https://doi.org/10.1016/j.mtcomm.2020.100955>.
- O.S. Es-Said, J. Foyos, R. Noorani, M. Mendelson, R. Marlloth, B.A. Pregger, Effect of layer orientation on mechanical properties of rapid prototyped samples, *Mater. Manuf. Process.* 15 (2000) 107–122, <https://doi.org/10.1080/10426910008912976>.
- A. Tsoukidas, M. Pantazopoulos, I. Katsoulis, D. Fasnakis, S. Maropoulos, N. Michailidis, Impact absorption capacity of 3D-printed components fabricated by fused deposition modelling, *Mater. Des.* 102 (2016) 41–44, <https://doi.org/10.1016/j.matdes.2016.03.154>.
- L. Wang, W.M. Gramlich, D.J. Gardner, Improving the impact strength of Poly lactic acid (PLA) in fused layer modeling (FLM), *Polymer* 114 (2017) 242–248, <https://doi.org/10.1016/j.polymer.2017.03.011>.
- W. Kuczko, F. Górska, R. Wichniarek, Impact strength of ABS parts manufactured using fused deposition modeling technology, *Arch. Mech. Technol. Autom.* 34 (2014) 3–12.
- M.Q. Tanveer, A. Haleem, M. Suhaib, Effect of variable infill density on mechanical behaviour of 3-D printed PLA specimen: an experimental investigation, *SN Appl. Sci.* 1 (2019) 1701, <https://doi.org/10.1007/s42452-019-1744-1>.
- J. Yi, R.F. LeBouf, M.G. Duling, T. Nurkiewicz, B.T. Chen, D. Schwegler-Berry, M. A. Virji, A.B. Stefanaki, Emission of particulate matter from a desktop three-dimensional (3D) printer, *J. Toxicol. Environ. Health Part A Curr. Issues*. 79 (2016) 453–465, <https://doi.org/10.1080/15287394.2016.1166467>.
- M. Pozuelo, F. Carréno, O.A. Ruano, Innovative ultrahigh carbon steel laminates with outstanding mechanical properties, *Mater. Sci. Forum* 426–432 (2003) 883–888, <https://doi.org/10.4028/www.scientific.net/msf.426-432.883>.
- V. Chellappa, B.Z. Jang, Crack growth and fracture behavior of fabric reinforced polymer composites, *Polym. Compos.* 17 (1996) 443–450, <https://doi.org/10.1002/pc.10632>.
- G. Biodegradability, Polymers Toughened Poly (lactic acid), BEP Composites with 1 (2019).**
- K. Bilge, S. Venkataraman, Y.Z. Menceloglu, M. Papila, Global and local nanofibrous interlayer toughened composites for higher in-plane strength, *Compos Part A Appl Sci Manuf* 58 (2014) 73–76, <https://doi.org/10.1016/j.compositesa.2013.12.001>.
- L. De Vivo, A.K. Matsushita, D. Kupor, J. Luna, B.A. Tierra, R.L. Sah, et al., Cholla cactus frames as lightweight and torsionally tough biological materials, *Acta Biomater.* 112 (2020) 213–224, <https://doi.org/10.1016/j.actbio.2020.04.054>.
- U.O. Costa, L.F.C. Nascimento, J.M. Garcia, W.B.A. Bezerra, S.N. Monteiro, Evaluation of Izod impact and bend properties of epoxy composites reinforced with mallow fibers, *J Mater Res Technol* 9 (2020) 373–382, <https://doi.org/10.1016/j.jmrt.2019.10.066>.
- M.A. Caminero, J.M. Chacón, I. García-Moreno, G.P. Rodríguez, Impact damage resistance of 3D printed continuous fibre reinforced thermoplastic composites using fused deposition modelling, *Compos. B Eng.* 148 (2018) 93–103, <https://doi.org/10.1016/j.compositesb.2018.04.054>.
- A. Pegoretti, I. Cristelli, C. Migliaresi, Experimental optimization of the impact energy absorption of epoxy-carbon laminates through controlled delamination, *Compos. Sci. Technol.* 68 (2008) 2653–2662, <https://doi.org/10.1016/j.compscitech.2008.04.036>.

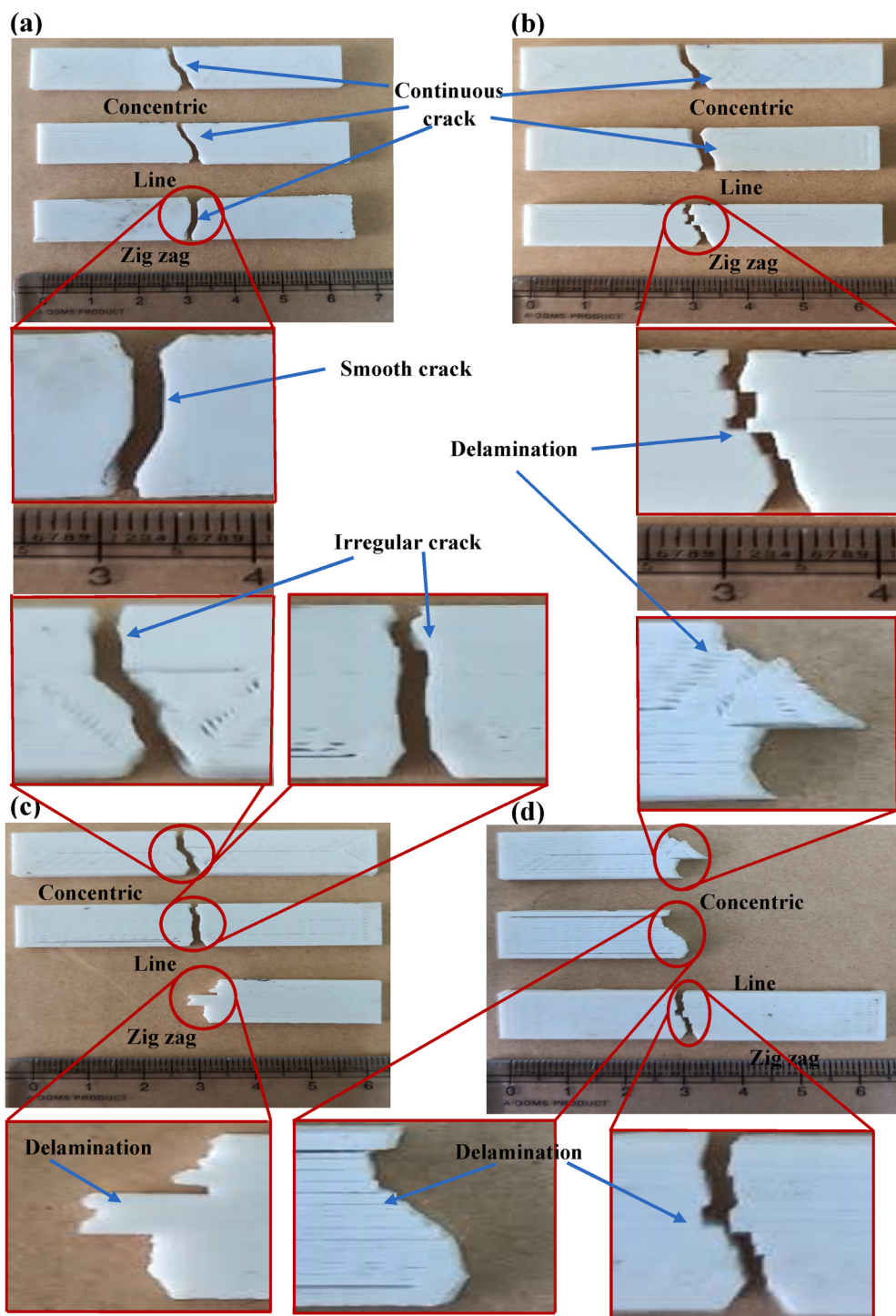


Fig. 5. Fracture behaviour of specimens after impact test at different infill density (a) 100% (b) 95% (c) 90% and (d) 85%.